Received: December 22, 2023; **Accepted:** June 29, 2024.
DOI. 10.30473/coam.2024.70032.1250
Summer-Autumn (2024) Vol. 9, No. 2, (67-83)
Research Article

Open Access

Control and Optimization in Applied Mathematics - COAM

Impact of Carrier Relaxation Time on the Performance of Quantum Dot Laser with Planar Cavities Using Artificial Neural Networks

Seyed Mohsen Izadyar[1], **Mohammad Eshaghnezhad**[2] ✉, **Hossein Davoodi Yeganeh**[3]

[1]Department of Physics, Faculty of Basic Sciences, Shahid Sattari University, Tehran, Iran.
[2]Department of Mathematics, Faculty of Basic Sciences, Shahid Sattari University, Tehran, Iran.
[3]Quantum Research Center, Shahid Sattari University, Tehran, Iran.

✉ **Correspondence:**
Mohammad Eshaghnezhad
E-mail:
m.eshaghnezhad@ssau.ac.ir

How to Cite
Izadyar, S.M., Eshaghnezhad, M., Davoodi Yeganeh, H. (2024). "Impact of carrier relaxation time on the performance of quantum dot laser with planar cavities using artificial neural networks", Control and Optimization in Applied Mathematics, 9(2): 67-83.

Abstract. This study presents a model of a quantum dot laser with a planar cavity, employing numerical methods and artificial neural networks for simulation purposes. The investigation focuses on the influence of critical parameters, including the injection current into the active layer of the quantum dot laser and the carrier relaxation time to a lower energy state level. The model delves into the intricate carrier and photon dynamics within the laser, solving a system of coupled equations that describe these interactions. The fourth-order Runge-Kutta method is utilized to solve these equations numerically. The results indicate that increased pumping power enhances the stable power levels and the peak power output of the laser. Additionally, analysis of the power versus intensity of current ($P-I$) characteristic curve reveals that a longer carrier relaxation time to a lower energy state leads to a higher threshold current and a reduction in the quantum efficiency of the device. The study also examines the laser switch-on time against the injection current. Finally, the deterioration in the quality of quantum dots and quantum wells is scrutinized. To gain deeper insights into the effect of increased pumping current on laser switch-on time, the study complements numerical findings with the application of artificial neural networks, yielding significant results.

Keywords. Quantum dot laser, Simulation, Differential equations, Laser dynamics, Artificial neural network.

MSC. 37N20, 65L06, 68T07.

1 Introduction

Quantum Dot (QD) semiconductor nanostructures have garnered significant interest among scientists over the past two decades due to their specific characteristics, which include their optical, electronic, and chemical properties [6, 20]. These nanostructures have found extensive applications in various fields such as television screens, laser active regions, optoelectronics devices, optical communications, light-emitting diodes $(LEDs)$, solar cells, biomedical and biological research , and chemical applications [2, 8, 10, 11, 14, 19, 24, 26, 32, 36, 37, 39, 43]. The Dirac delta-like density of states, a result of the confinement of carrier motion in all three dimensions, is responsible for these distinctive properties and applications of QDs. This confinement leads to a discontinuity in the state density and the formation of discrete energy states, causing QDs to behave similarly to atoms. Consequently, they are often referred to as "artificial atoms" in some literature [21, 23].The theoretical prediction of QDs being used as the active layer in lasers was first proposed in the early 1980's [1], owing to their higher gain of QDs compared to quantum wells (QWs). However, the complexity of the fabrication process led to a decade-long hiatus in QD laser research until the first experimental demonstration of self-assembled quantum dot lasing in 1994 [22]. This breakthrough opened the door to further developments in QD laser technology. QD lasers have improved the performance of semiconductor lasers in numerous aspects, including reduced threshold currents, enhanced quantum efficiency, narrower spectral linewidth, faster modulation speed, improved temperature stability of the threshold current, increased optical gain, applications in nonlinear optics, etc. [7, 9, 15, 16, 17, 25, 27, 28, 35].

InAs/GaAs quantum dot lasers operating at a wavelength of 1.3 μm have extensive applications in optical communication, telecommunications, photonic quantum technology, and as near-infrared broadband light sources [18, 29, 33, 34]. In this study, a QD laser with a dot-in-well (DWELL) structure, composed of InAs/GaAs, is modeled and simulated using numerical methods and neural networks.

Neural networks, with their ability to generalize and learn from data, can serve as a suitable alternative substitute to traditional numerical methods. Their rapid computation time makes them ideal for implementing complex functions across different domains. Various neural networks have been employed to solve linear and non-linear first-order differential equations [5, 31, 38]. Unlike classical methods, neural networks do not require an initial condition to solve first-order differential equations. They achieve convergence through the training of arbitrary weights [4]. This capability is one of the key advantages of the neural network advantages. The most widely used neural networks are error backpropagation networks. Error backpropagation networks, which are multi-layer networks, are particularly effective for prediction and classification tasks. In this paper, the error backpropagation network is theoretically introduced and utilized to solve a set of first-order equations.

The modeling and simulation of the InAs/GaAs QD laser in a DWELL structure are carried out using a system of coupled equations for the ground state (GS), excited states (ESs), wetting layer (WL), and separate confinement heterostructures (SCH) layer. The behavior of carrier and photon densities is described by a set of time-dependent amalgamated differential equations. The SCH layer and WL contribute to the pumping process, while the two excited states and GS are involved in carrier dynamics and the lasing process. For the sake of simplicity, it is assumed that each QD has an identical shape and size, and the effects of homogeneous and inhomogeneous broadening are neglected. The gain

spectrum is assumed to be its maximum value. The coupled equations are solved numerically using the fourth-order Runge-Kutta method [3].

The objective of this paper is to investigate the dynamic influence of carriers on the performance of QD laser and how this changes with different carrier relaxation times in the GS. By solving the coupled equations and analyzing the output data, valuable insights such as the output power of the laser, the $P-I$ (power versus intensity of current) characteristic curve for the three energy states involved in lasing, and the $P-I$ curve for the ground state at varying relaxation and carrier recombination times are obtained. Finally, error backpropagation networks are employed to enhance the prediction of the laser response to current injection at different intervals and to assess the impact of relaxation time on the laser performance.

2 Carrier and Photon Dynamics and Equations

Figure 1 (a) presents a schematic of the simulated laser cavity with a planar waveguide. The InAs columnar-shaped quantum dots are grown on an (001) n-type GaAs substrate, known as the wetting layer (WL), using the self-assembled QD stacking method and Stranski-Krastanov mode, facilitated by molecular beam epitaxy (MBE). These QDs islands on the WL are sandwiched between two other layers: GaAs-type SCH and Al0.4Ga0.6As cladding layers [41]. The active region of the QD laser consists of ten layers of QD, each with a width of 4 μm and a monolayer height of 8 nm, and the device operates at room temperature.

The dynamics of carriers and photons in the laser active region can be modeled numerically using a comprehensive set of coupled equations. The QD active region comprises five energy states: two states (WL and SCH) are responsible for the pumping and diffusion of electron-hole pairs, and the other three levels (GS, $ES1$, and $ES2$) are involved in the leasing processes within the cavity. For simplicity, the time dependency of the current injection is assumed to be constant, meaning that a precise amount of electrons per unit time is pumped into the active region of the laser. This injection or pumping process increases the number of electron-hole pairs in the device (electrons in the conduction band (CB) and holes in the valance band (VB)). Figure 1 (b) illustrates the band diagram of the InAs/GaAs QD laser active region in the CB [3]. The processes that occur to carriers, specifically electrons in the CB are also depicted. It is assumed that charge neutrality is always preserved within each quantum dot. Each electron-hole pair is referred to as an exciton. Using the excitonic approximation, every process that occurs to electrons in the CB will also occur for holes in the VB, so only CB is considered for modeling purposes.

Each process shown in Figure 1 (b) is associated with a time constant. These time constants include τSCH for carrier diffusion from the SCH, τ_{sr} for carrier recombination in the SCH (decay time), τ_{eWL} for carrier escape from the WL to the SCH, τ_c for carrier relaxation from the quantum well to the dot, τ_e for carrier escape from the quantum dot to the well, τ_{qr} for carrier recombination in the WL, τ_0 for relaxation time within QD states, τ_r for carrier recombination within QD and τ_s for photon lifetime.

Upon turning on the laser, the injection current is pumped into the SCH, increasing the electron-hole pairs or carrier density in the SCH. The injected carriers into the SCH relax to the WL (τ_{SCH}) and undergo another fast relaxation from the WL to $ES2$ (τ_c). Most carriers are captured by $ES2$,

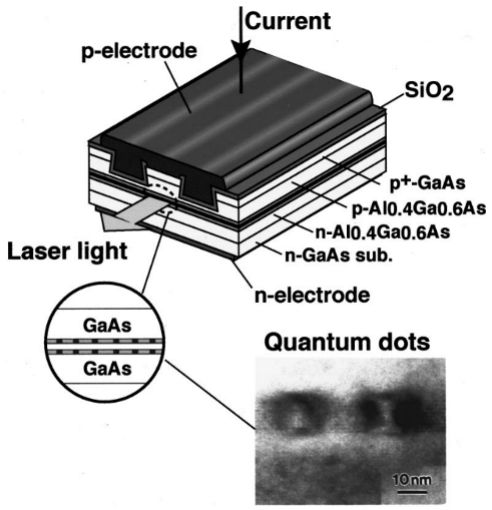

(a) The QD laser cavity and TEM image of columnar shaped QDs [41].

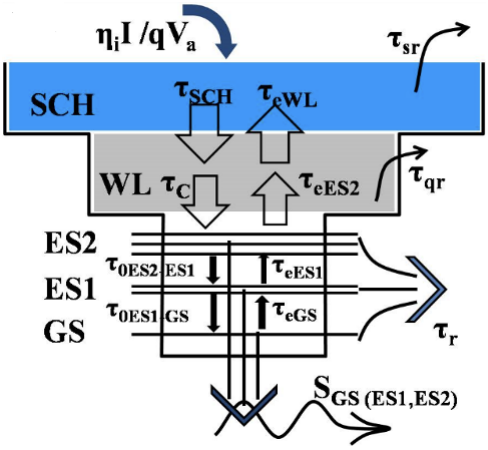

(b) Simplified schematic of band diagram with energy states of CB for InAs/GaAs self-assembled QD laser.

Figure 1: The QD laser structure

some carriers decay (τ_{qr}), and several carriers escape from $ES2$ to the WL (τ_{eES2}). The processes that carriers experience in the GS, $ES1$, and $ES2$ are similar, so only $ES1$ is taken into account for interpretation. A few carriers relax from $ES2$ to $ES1$ ($\tau_{0ES2-ES1}$) and a few carriers relax into the GS from $ES1$ ($\tau_{0ES1-GS}$). Additionally, parts of carriers that escape from the GS are captured by the $ES1$ (τ_{eGS}) and by $ES2$ (τ_{eSE1}). Some carriers decay through spontaneous recombination and Auger effects (τ_r). The remaining carriers contribute to the induced emission to produce photons. The ratio of the injection current to the emitted photon is defined as the quantum efficiency.

By analyzing the carrier dynamics in QDs, a numerical model of the QD laser is constructed using a set of coupled equations. This model can be introduced by two groups of time-dependent equation: carrier equation (Equations (1)-(5)) and photon equations (Equations (6)-(8)) as follows:

$$\frac{dN_{SCH}}{dt} = \eta_i \frac{I}{qV_a} - \frac{N_{SCH}}{\tau_{SCH}} - \frac{N_{SCH}}{\tau_{sr}} + \frac{N_{WL}}{\tau_{eWL}}, \tag{1}$$

$$\frac{dN_{WL}}{dt} = -\frac{N_{WL}}{\tau_{qr}} + \frac{N_{SCH}}{\tau_{SCH}} + \frac{N_{ES2}}{\tau_{eES2}} + \frac{N_{WL}}{\tau_{eWL}}(1 - f_{ES2}), \tag{2}$$

$$\begin{aligned}\frac{dN_{ES2}}{dt} = &-\frac{N_{ES2}}{\tau_r} - \Gamma\nu_g g_{ES2}(2f_{ES2} - 1)S_{ES2} - \frac{N_{ES2}}{\tau_{eES2}} + \frac{N_{WL}}{\tau_c}(1 - f_{ES2}) \\ &- \frac{N_{ES2}}{\tau_{0ES2-ES1}}(1 - f_{ES1}) + \frac{N_{ES1}}{\tau_{eES1}}(1 - f_{ES2}),\end{aligned} \tag{3}$$

$$\begin{aligned}\frac{dN_{ES1}}{dt} = &-\frac{N_{ES1}}{\tau_r} - \Gamma\nu_g g_{ES1}(2f_{ES1} - 1)S_{ES1} + \frac{N_{GS}}{\tau_{eGS}}(1 - f_{ES1}) \\ &- \frac{N_{ES1}}{\tau_{0ES1-SG}}(1 - f_{GS}) + \frac{N_{ES2}}{\tau_{0ES2-ES1}}(1 - f_{ES1}) - \frac{N_{ES1}}{\tau_{eES1}}(1 - f_{ES2}),\end{aligned} \tag{4}$$

$$\frac{dN_{GS}}{dt} = -\frac{N_{GS}}{\tau_r} - \Gamma\nu_g g_{GS}(2f_{GS} - 1)S_{GS} - \frac{N_{GS}}{\tau_{eGS}}(1 - f_{ES1})$$

$$+\frac{N_{ES1}}{\tau_{0ES1-GS}}(1-f_{GS}), \tag{5}$$

$$\frac{dS_{GS}}{dt}=-\frac{S_{GS}}{\tau_s}+\Gamma\nu_g g_{GS}(2f_{GS}-1)S_{GS}+\beta_{sp}\frac{N_{GS}}{\tau_{sp}}, \tag{6}$$

$$\frac{dS_{ES1}}{dt}=-\frac{S_{ES1}}{\tau_s}+\Gamma\nu_g g_{ES1}(2f_{ES1}-1)S_{ES1}+\beta_{sp}\frac{N_{ES1}}{\tau_{sp}}, \tag{7}$$

$$\frac{dS_{ES2}}{dt}=-\frac{S_{ES2}}{\tau_s}+\Gamma\nu_g g_{ES2}(2f_{ES2}-1)S_{ES2}+\beta_{sp}\frac{N_{ES2}}{\tau_{sp}}, \tag{8}$$

where S_{GS}, S_{ES1} and S_{ES2}, are the photon densities in the GS, $ES1$, and $ES2$, respectively. N_{SCH}, N_{WL}, N_{ES2}, N_{ES1} and N_{GS} are the carrier densities in the SCH, WL, $ES2$, $ES1$, and GS, respectively. Note that in the excitonic model, the number of electrons in the CB and the number of holes in the VB are exactly equal. η_i is the injection current rate, I is the injection current and q is the unit charge. Terms like -$-\frac{N_{GS}}{\tau_r}$, $-\frac{N_{ES1}}{\tau_r}$, $-\frac{N_{ES2}}{\tau_r}$, $-\frac{N_{WL}}{\tau_{qr}}$ and $-\frac{N_{SCH}}{\tau_{sr}}$ are decay rates of carriers in GS, $ES1$, $ES2$, WL, and SCH, respectively . Terms like $-\frac{N(1-f)}{\tau_e}$ represent the rate of carriers escaping from the present state to the upper one. Terms $\frac{N(1-f)}{\tau_0}$ and $-\frac{N(1-f)}{\tau_0}$ show the relaxation rate of carriers from the upper state into the present one and from the present state into the lower one, respectively. The parameter f indicates the occupation probability of an individual state. Furthermore, the term $-\frac{N_{WL}(1-f_{ES})}{\tau_c}$ is the rate of carrier relaxation from the WL to $ES2$. $-\frac{S_{GS}}{\tau_s}$, $-\frac{S_{ES1}}{\tau_s}$ and $-\frac{S_{ES2}}{\tau_s}$ are photon decay rates. Terms $\beta_{sp}\frac{N_{GS}}{\tau_{sp}}$, $\beta_{sp}\frac{N_{ES1}}{\tau_{sp}}$ and $\beta_{sp}\frac{N_{ES2}}{\tau_{sp}}$ are photon production rates due to the spontaneous recombination, where β_{sp} is the spontaneous emission coupling factor, and τ_{sp} is the spontaneous recombination time. Finally, $\Gamma\nu_g g_{GS}(2f_{GS}-1)S_{GS}$, $\Gamma\nu_g g_{ES1}(2f_{ES1}-1)S_{ES1}$ and $\Gamma\nu_g g_{ES2}(2f_{ES2}-1)S_{ES2}$ depict the photon production and carrier recombination rates by the stimulated emission of radiation, where ν_g is the group velocity, Γ is the optical confinement factor, and g is the maximum gain of QDs. It is worth mentioning that the positive terms denote an increase in carriers or photons, and negative terms denote a decrease in N and S.

When carriers transfer from one state to another, they are influenced by Pauli's exclusion principle. The parameter f denotes the occupation probability of the entrance state. Therefore, f_{GS}, f_{ES1}, and f_{ES2} represent the occupation probability of carriers in GS, $ES1$, and $ES2$, respectively. It can be expressed as:

$$f=\frac{N}{\mu N_D}, \tag{9}$$

where N is the density of state for each state, N_D is the total number of QDs, and μ is the degeneracy. The degeneracy of the GS, $ES1$, and $ES2$ is 2, 4, and 6, respectively [29].

All parameters in the rate equations play a role in the operation of the QD laser. However, certain parameters are particularly influential in the dynamics of carriers and photon. Among these, the injection current and carrier relaxation times are the primary focus of this paper. The impact of these parameters on the QD working condition is discussed in detail in the subsequent section.

The model presented in this section is simulated using numerical methods for solving equations. An alternative model based on artificial neural networks will be introduced later in the paper. Our previous study [3] utilized these rate equations to simulate the QD laser. Here, we follow the same procedure and obtain new insights into how carrier relaxation times affect laser performance. Additionally, we also use a novel simulation method employing artificial neural networks to model the QD laser. The outcomes from both methods will be compared and discussed thoroughly.

3 Results and Discussions

The system of equations, Equations (1)-(8), involves eight interrelated variables. These equations are solved numerically using the fourth-order Runge-Kutta method. The resulting output provides insights into the dynamics of photon and carrier densities in each state, allowing for an analysis of the laser operational behavior. Various interpretations can be derived from these results, including the laser response to a stepped injection current, the output power of the GS, $ES1$, and $ES2$, $P-I$ characteristic, turning-on time, etc. Some parameters used in the simulation are listed in Table 1.

Table 1: Parameters Used in the simulation [3, 29, 41]

Parameter	Notation	Value
Cavity Length	L	1000m
Refractive index	n_r	3.5
Reflectivity of Output Mirror	R_1	0.3
Reflectivity of Another Mirror	R_2	0.9
Reflectivity of Another Mirror	R_2	0.9
Energy Gap between WL and $ES2$	Δ_{WL-ES2}	0.0128eV
Energy Gap between $ES1$ and $ES2$	$\Delta_{ES2-ES1}$	0.0360eV
Energy Gap between $ES1$ and GS	Δ_{ES1-GS}	0.0370eV
Energy of Each Photon of GS	ν	0.9644eV
Spontaneous Emission Coupling Factor	β_{sp}	10^{-7}
Injection Current Rate	γ_i	0.9
Optical Confinement Factor	Γ_i	0.1
Peak Gain of GS	g_{GS}	$25.38 \times 10^{-4}\mu m^{-1}$
Peak Gain of $ES1$	g_{ES1}	$437.58 \times 10^{-4}\mu m^{-1}$
Peak Gain of $ES2$	g_{ES2}	$455.30 \times 10^{-4}\mu m^{-1}$
Group Velocity	ν_g	$8.571 \times 10^{4}\mu m/ns$
Temperature	T	$293K$
QD Density	N_D	$4.3 \times 10^{22}m^{-3}$

The findings from the modeling the InAs/GaAs self-assembled QD laser are presented below.

3.1 Numerical simulation results and laser response to injected current

Figure 2 (a) illustrates the laser output power of GS as a function of time for various injection currents. The laser switch-on time is determined by this curve as the time when the laser output power reaches half of its maximum value [3]. Furthermore, the laser stability time is defined as the point at which the output power reaches a steady state with no further relaxation oscillation. As observed, an increase in

the injection current leads to a reduction in both the laser switch-on time and the laser stability time, as well as an increase in the power peak and the achievable steady power. For injection currents exceeding 50 mA, the QD laser becomes saturated. This means that further increases in the input injection current do not result in higher steady-state power, but rather lead to an increase in the switch-on time and power peak. Figure 2 (a) is consistent with findings reported in the literature [30].

Figure 2 (b) displays the $P-I$ characteristic curve for the three energy states involved in the lasing process . This curve is a crucial and practical indicator of the laser operational behavior. It provides the output power of the laser as a function of the input injection current into the active layer. From this curve, one can determine the threshold current, the efficiency dP/dI, the external quantum efficiency, and the saturation current.

The threshold current is defined as the injection current at which the $P-I$ curve begins to behave as a constant function. To excite higher energy states, a greater injection current is necessary to populate these states with active carriers. Consequently, these upper states emit photons at higher threshold currents. As shown in Figure 2 (b), upon injection of current, the GS begins to emit photons. Once the GS is saturated, $ES1$ starts to emit photons, and after $ES1$ saturation, electron-hole pairs in $ES2$ recombine and emit photons through stimulated emission. The threshold currents for the GS, $ES1$, and $ES2$ are 9, 45, and 238 mA, respectively. It is important to note that a high injection current can damage the active layer and lead to laser failure.

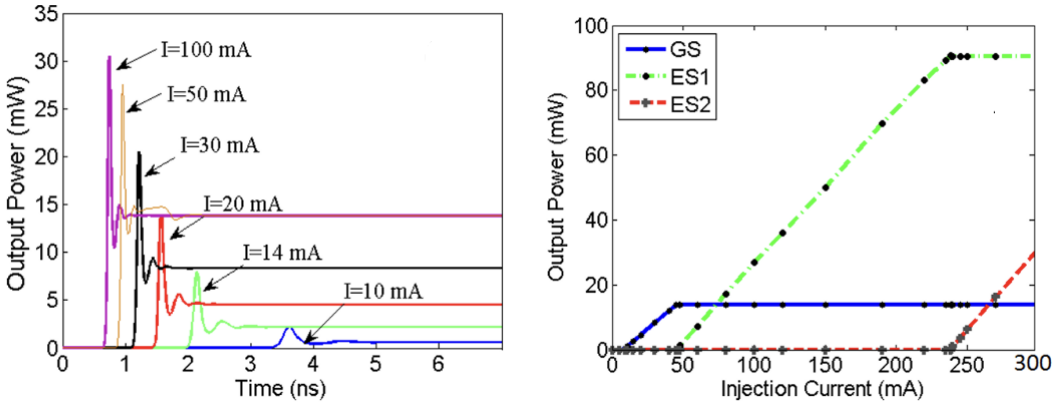

(a) Output laser power in GS at different injection currents. **(b)** $P-I$ characteristic curve of GS, $ES1$, and $ES2$ [3].

Figure 2: Power characteristic of QD laser

Figure 3 depicts the $P-I$ curve for the GS under various carrier relaxation times from $ES1$ to GS. Given that the threshold currents for $ES1$ and $ES2$ are high (as shown in Figure 2 (b)) and could potentially damage cavity elements in an experimental setup, only the GS output is presented in Figure 3. Parameters utilized in the model are detailed in Table 1. The $P-I$ curve is computed for different recombination lifetimes: (a) $\tau_r = 2.8ns$ and $\tau_{qr} = 3ns$, (b) $\tau_r = 2.8ns$ and $\tau_{qr} = 0.5ns$ and (c) $\tau_r = 1ns$ and $\tau_{qr} = 0.5ns$. Figure 3 (a) corresponds to a high-quality QD and QW, Figure 3 (b) to a high-quality QD and a low-quality QW, and Figure 3 (c) to a low-quality QD and QW.

Despite the Dirac delta-like density of states in QD leading to high (differential) optical gain, retardation of carrier relaxation into QD energy states is one of the limitations in the design of QD lasers. This delay is due to state filling, which is a consequence of the exclusion principle, and the requirement

for energy conservation. This issue is known as the phonon bottleneck problem[42, 44]. However, this problem has been largely addressed in recent years, and various methods have been proposed to facilitate the rapid relaxation of carriers into QDs [40]. Consequently, experimentally reported relaxation times have been incorporated into these result.

As shown in Figure 3 (a), an increase in the carrier relaxation time to the GS leads to a reduction in quantum efficiency and an increase in threshold current. It is also evident that for a constant injection current, the laser output power decreases. This behavior is attributed to carriers residing in higher energy levels for a longer duration at larger relaxation times, which increases the likelihood of the carriers decay through spontaneous and non-radiative recombination in these levels. As a result, more energy is required to increase the carriers population to achieve lasing. It is also observed that for larger relaxation times, the curve remains unchanged after a certain current, indicating that the ground state saturates earlier at higher τ_{0s}.

In Figure 3 (b), the impact of increasing the relaxation time on the $P-I$ characteristic becomes more pronounced as the carrier recombination time in the quantum well decreases (indicative of a low-quality quantum well). A reduction in τ_{qr} increases the probability of non-radiative recombination in carriers outside the dots, and leading to an increase in threshold current due to the enhanced carrier dissipation in the QD through non-radiative processes. When both the QD and the QW are of low quality (as in Figure 3 (c), where recombination times are reduced), the increase in the threshold current becomes significant due to the prolonged relaxation time of carriers into the lasing state. This effect is a result of carrier decay in the QDs. This scenario holds true even for rapid carrier relaxations into the GS. It is important to note that an increase in injection current leads to an increase in carriers within the SCH barrier layer (N_{SCH}, followed by an increase in carriers within the wetting layer N_q, resulting in more carriers relaxing into QDs and participating in the leasing process.

The dependency of τ_q, and thus the dependency of QW crystal quality on the threshold current and the external quantum efficiency, is due to the delayed carrier relaxation, which increases the opportunity for carriers to recombine through the non-radiative process outside the dots [40].

Figure 4 depicts the relationship between the laser switch-on time and the injected current at different relaxation times of the GS. This graph is plotted for three scenarios: (a) high-quality QD and QW, (b) high-quality QD and low-quality QW, and (c) low-quality QD and QW. The laser switch-on time exhibits an exponential behavior and is consistent with findings reported in the literature [7, 12]. As observed in Figure 4, an increase in the relaxation time leads to an increase results in a prolonged laser switch-on time for a given injection current. This is because, at a certain current, a longer relaxation time implies that carriers remain in the upper states for a longer duration, consequently delaying the laser turn-on. As anticipated, a reduction in the QW quality leads to a later turn-on of the laser. Furthermore, a decrease in the QD quality increases the separation between the graphs at different τ_0 times, indicating an even longer laser switch-on time. The rapid turn-on of a laser is a critical factor in high-speed modulation and the modulation response of semiconductor lasers [30].

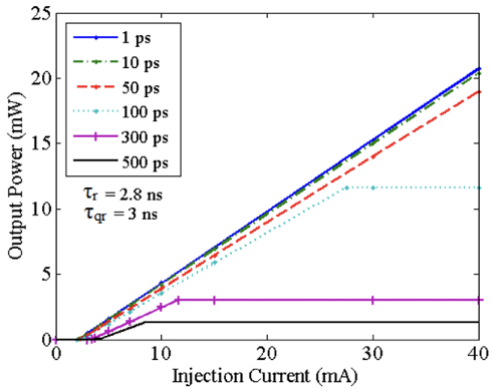

(a) $P-I$ characteristic curve for $\tau_r = 2.8ns, \tau_{qr} = 3ns$.

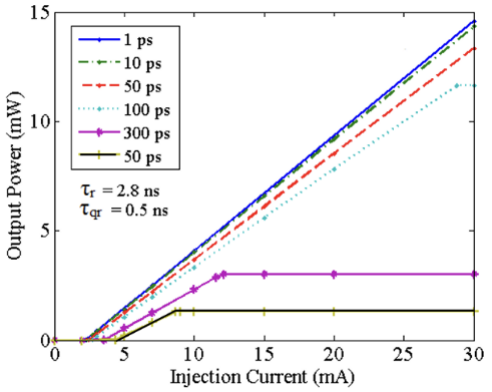

(b) $P-I$ characteristic curve for $\tau_r = 2.8ns$, $\tau_{qr} = 0.5ns$.

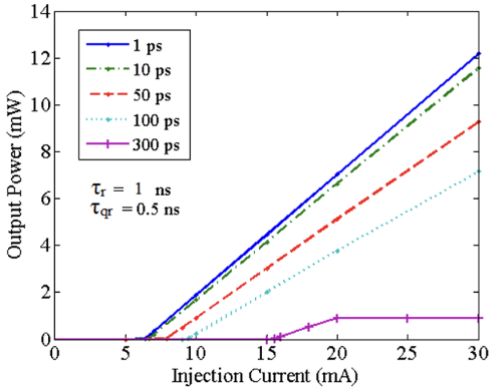

(c) $P-I$ characteristic curve for $\tau_r = 1ns$ and $\tau_{qr} = 0.5ns$.

Figure 3: $P-I$ characteristic curve

3.2 Artificial neural network

Artificial neural networks ($ANNs$) are composed of interconnected, nonlinear processor elements. These networks consist of individual processor elements that work together to solve a problem. The processing element of an ANN operates in two phases: the learning phase and the application phase. During the learning phase, the processor element learns to activate for a specific state. In the application phase, when a trained input pattern is recognized, the corresponding output is generated. If the input pattern does not match any of the previously taught patterns, activation rules determine whether the output of the cell is activated. In summary, an artificial neural network is a computational method based on the interconnected elationships of multiple processing units. The network is made up of an arbitrary number of cells, nodes, units or neurons that link the input set to the output. While artificial neural networks are not comparable to natural neural systems, they possess capabilities that make them unique in certain applications, such as pattern separation, robotics, control systems, and generally in scenarios where learning linear and non-linear mapping is required. A general form of the mathematical interpretation of neural networks is presented in Figure 5.

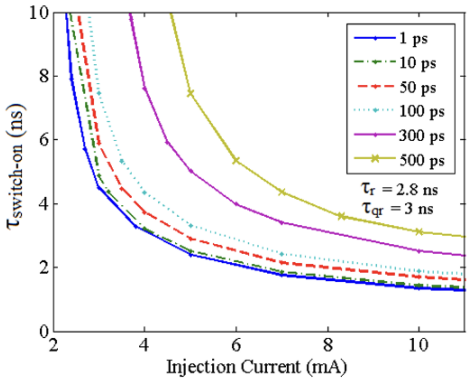

(a) laser switch-on time in terms of injected current for $\tau_r = 2.8ns$, $\tau_{qr} = 3ns$.

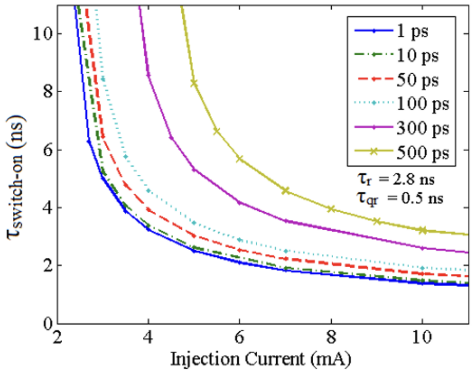

(b) laser switch-on time in terms of injected current for $\tau_r = 2.8ns$, $\tau_{qr} = 0.5ns$.

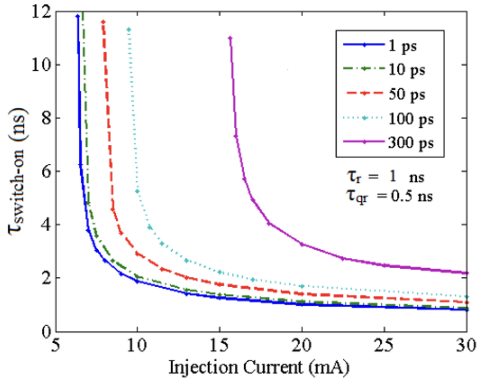

(c) laser switch-on time in terms of injected current for $\tau_r = 1ns$ and $\tau_{qr} = 0.5ns$.

Figure 4: Laser switch-on time

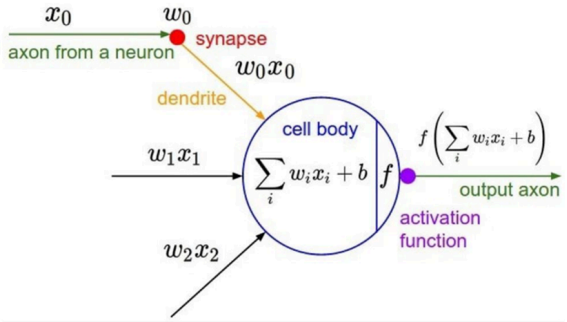

Figure 5: Conventional mathematical model [13].

Feedforward multilayer neural network with backpropagation

In our investigation, A feedforward multi-layer network is structured with layers of neuron, typically with full connectivity between neurons of adjacent layers. Such networks, known as Multilayer Feedforward

Networks (FFN), have proven effective in tackling a wide range of learning and classification tasks. Training these networks often involves the application of various learning algorithms A prevalent choice among these is the backpropagation algorithm, which is a supervised learning method. This algorithm employs gradient descent to minimize the mean squared error between the network output and the desired output. Once the network error is reduced to a predetermined threshold level, the network is considered to have converged. In this study, we have modeled the data in two cases to forecast the laser response to current injection over varying intervals and to assess the impact of time on this response. The Figure 6 illustrates the inputs and outputs for these two cases.

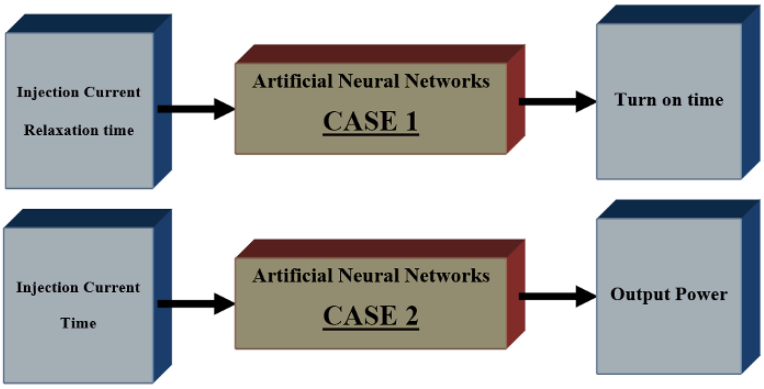

Figure 6: Inputs and outputs for two cases.

To model each case, a multi-layer feedforward network equipped with an error backpropagation algorithm has been employed. This network is characterized by an input layer, a hidden layer, and an output layer, constituting a three-layer network architecture. Multiple configurations have been explored to model this network, with the primary difference among these configurations being the number of neurons and the transfer functions utilized in the hidden layers. Table 2 presents the range of neurons and transfer functions used in the hidden layers to generate and train different network configurations.

Table 2: Range of neurons and transfer functions used in the hidden layers

Transfer function of layer2	Neuron of layer 2	Transfer function of layer 1	Neuron of layer 1
Tansig Logsig Satlin Satlins	2-12	Tansig Logsig Satlin Satlins	2-12

As indicated in Table 2, the number of neurons employed in the first and second layers fluctuates from 2 to 12. Furthermore, a single neuron is utilized in the third layer, which is the output layer. Additionally, this algorithm explores various transfer functions. The transfer functions for the input and hidden layers include Tansig, Logsig, Satlin, and Satlins. Moreover, the transfer function for the

output layer is Purelin. Finally, the Trainlm training method is employed for network training. In the error backpropagation algorithm, laboratory data is utilized randomly to obtain the solution of equations (1)-(8). This data is divided into three categories: training data (60%), validation data (20%), and testing data (20%). The training data serves to correct and adjust weights and biases. The validation data is employed to validate the trained network. Finally, the testing data is used to evaluate the network. Following the training of different networks for each case, a structure from each case that exhibits higher accuracy and superior results is chosen. Table 3 displays the specifications of this structure for both cases 6. These models are selected based on the $R-square$ parameter. The values of $R-square$ parameters are also listed in Table 3.

Table 3: Specifications of the structure for two cases

Transfer function of layer2	Neuron of layer 2	Transfer function of layer 1	Neuron of layer 1.
Tansig Logsig Satlin Satlins	2-12	Tansig Logsig Satlin Satlins	2-12

In Figure 7(a), the laser response to varying injection currents is depicted over the specified time frame. This figure has been generated using the neural networks method and corresponds to Figure 2(a). Through the application of neural networks, the laser output power is calculated for a continuous range of injected currents. Figure 7(b) presents a top view of Figure 7(a). As anticipated, it is evident in Figure 7(b) that the laser turn-on time decreases exponentially with an increase in the injection current.

To gain a deeper insight into the variation of the laser switch-on time with changes in the carrier relaxation time to a lower state, Figure 8 has been extracted using artificial neural networks. This figure illustrates the laser switch-on time across different injection currents and relaxation times. It serves as a 3D counterpart to Figure 4 (a). As observed and expected, an increase in the relaxation time leads to a noticeable rise in the laser switch-on time. Additionally, it is apparent that an increase the injection current results in a decrease in the switch-on time, due to the rapid occupation of the upper energy state by the carriers. The advantage of this result over Figure 4 (a) lies in its continuous representation and swift computational cycle. The principal advantages of the artificial neural networks method over the Runge-Kutta method can be explained as follows:

1. The Runge-Kutta method requires initial values to solve the rate equations (Equations (1)-(8)), and for accurate calculations, the model must execute in a correct physical context, running at least one cycle to determine the true initial values. This process can be time-consuming and complex. In contrast, neural networks employ arbitrary weights to model the laser, eliminating the need for initial values.

2. The neural networks method can produce results with continuous variables in a short time.

3. Optimization of the desired laser parameters is more straightforward with the neural networks method compared to numerical methods such as Runge-Kutta.

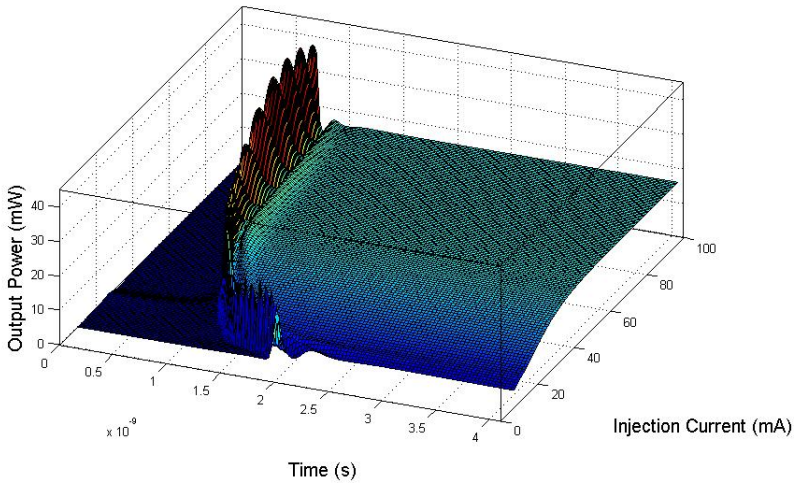

(a) Output power of the QD laser versus time and injected current, derived using the neural networks method.

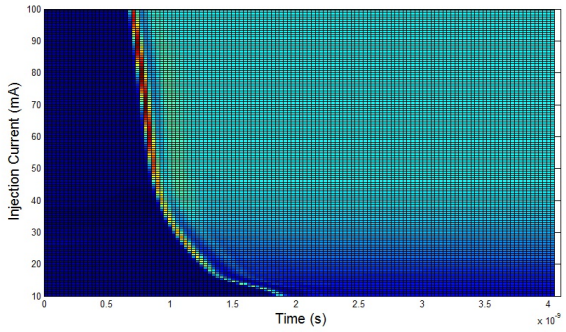

(b) Top view of the laser switch-on time, corresponding to (a).

Figure 7: Results from the artificial neural network method for the QD laser

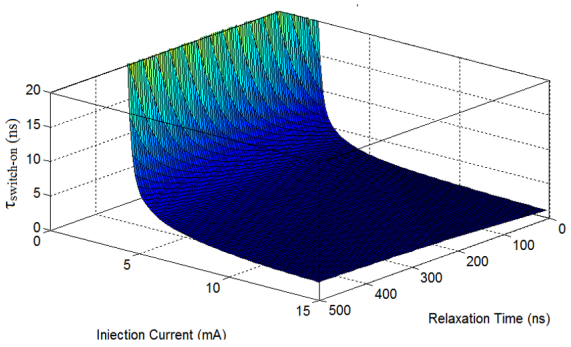

Figure 8: Laser switch-on time versus injected current and carrier relaxation time, obtained using the neural network.

4 Conclusion

In this paper, we have proposed a model for the QD laser based on a set of governing equations. The QD compound was InAs/GaAs. We have conducted a comprehensive investigation into the dynamics of carriers and photons. The impact of critical parameters such as injection currents and relaxation times of carriers to lower energy states has been thoroughly examined and analyzed. The system of coupled equations was solved numerically using the fourth-order Runge-Kutta method. Through the analysis of the numerical solutions, we have presented and interpreted various findings. Notable results include the laser performance under stepped injection current, the $P-I$ characteristic curve for states involved in lasing, the $P-I$ characteristic curve for the ground state GS at varying relaxation and recombination times, and the laser switch-on time as a function of injected current at different relaxation times for three cases: high-quality QD and QW, high-quality QD and low-quality QW, and low-quality QD and QW. We observed that with the increase of as the injection current increases, the laser switch-on time and stability time decrease, while the maximum and stable powers increase. The power increase of continues until the photon emission in each energy state reaches to steady state. Once emission stability is achieved in each energy state, the upper energy state begins to contribute to the output power of the device. Additionally, we found that an increase in the relaxation time leads to a higher threshold current a lower quantum efficiency, a longer laser switch-on time, and a reduction in both the achievable stable power and the power peak. Furthermore, A decrease in the quality of quantum dots and wells was also found to diminish the device efficiency. Utilizing the artificial neural networks method, we have explored the response of the laser to a continuous range of the injection currents and demonstrated the exponential relationship between the laser switch-on time and the injection current in a novel way. Furthermore, the impact of relaxation time on the laser turn-on visualized using this method. Lastly, we have discussed the advantages of the neural networks method over the Runge-Kutta method.

Declarations

Availability of Supporting Data

All data generated or analyzed during this study are included in this published paper.

Funding

The authors conducted this research without any funding, grants, or support.

Competing Interests

The authors declare that they have no competing interests relevant to the content of this paper.

Authors' Contributions

The main text of manuscript is collectively written by the authors.

References

[1] Asada, M., Miyamoto, Y., Suematsu, Y. (1986). "Gain and the threshold of three-dimensional quantum-box lasers", IEEE Journal of Quantum Electronics, 22, 1915-1921.

[2] Azam, N., Najabat Ali, M., Javaid Khan, T. (2021). "Carbon quantum dots for biomedical applications: Review and analysis", Frontiers in Materials, 8, 700403.

[3] Daraei, A., Izadyar, S.M., Chenarani, N. (2013). "Simulation and analysis of carrier dynamics in the inas/gaas quantum dot laser, based upon rate equations", Optics and Photonics Journal, 3.

[4] Effati, S., Mansoori, A., Eshaghnezhad, M. (2021). "Linear quadratic optimal control problem with fuzzy variables via neural network", Journal of Experimental & Theoretical Artificial Intelligence, 33, 283-296.

[5] Eshaghnezhad, M., Rahbarnia, F., Effati, S., Mansoori, A. (2019). "An artificial neural network model to solve the fuzzy shortest path problem", Neural Processing Letters, 50, 1527-1548.

[6] Facure, M., Schneider, R., Mercante, L., Correa, D. (2020). "A review on graphene quantum dots and their nanocomposites: From laboratory synthesis towards agricultural and environmental applications", Environmental Science Nano, 7.

[7] Fathpour, S., Zetian Mi, Bhattacharya, P. (2005). "High-speed quantum dot lasers", Journal of Physics D: Applied Physics, 38, 2103.

[8] Filali, S., Pirot, F., Miossec, P. (2020). "Biological applications and toxicity minimization of semiconductor quantum dots", Trends in Biotechnology, 38, 163-177.

[9] García de Arquer, F.P., Talapin, D.V., Klimov, V.I., Arakawa, Y., Bayer, M., Sargent, E.H. (2021). "Semiconductor quantum dots: Technological progress and future challenges", Science, 373.

[10] Ghaffarkhah, A., Hosseini, E., Kamkar, M., Sehat, A.A., Dordanihaghighi, S., Allahbakhsh, A., van der Kuur, C., Arjmand, M. (2022). "Synthesis, applications, and prospects of graphene quantum dots: A comprehensive review", Small, 18, 2102683.

[11] Ghosh, D., Sarkar, K., Devi, P., Kim, K. H., Kumar, P. (2021). "Current and future perspectives of carbon and graphene quantum dots: From synthesis to strategy for building optoelectronic and energy devices", Renewable and Sustainable Energy Reviews, 135, 110391.

[12] Ghosh, S., Bhattacharya, P., Stoner, E., Singh, J., Jiang, H., Nuttinck, S., Laskar, J. (2001). "Temperature-dependent measurement of Auger recombination in self-organized In 0.4 Ga 0.6 As/GaAs quantum dots", Applied Physics Letters, 79, 722-724.

[13] Gupta, R.R., Ranga, V. (2021). "Comparative study of different reduced precision techniques in deep neural network", In Proceedings of International Conference on Big Data, Machine Learning and their Applications: ICBMA 2019, 123-136.

[14] Gidwani, B., Sahu, V., Shukla, S.S., Pandey, R., Joshi, V., Jain, V.K., Vyas, A. (2021). "Quantum dots: Prospectives, toxicity, advances and applications", Journal of Drug Delivery Science and Technology, 61, 102308.

[15] Izadyar, S.M., Razaghi, M., Hassanzadeh, A. (2017). "Quantum dot semiconductor optical amplifier: Role of second excited state on ultrahigh bit-rate signal processing", Applied Optics, 56, 3599-3607.

[16] Izadyar, S.M., Razaghi, M., Hassanzadeh, A. (2018). "Quantum dot semiconductor optical amplifier: Investigation of amplified spontaneous emission and noise figure in the presence of second excited state", Optical and Quantum Electronics, 50, 1-13.

[17] Izadyar, S.M., Razaghi, M., Hassanzadeh, A. (2020). "Quantum dot semiconductor optical amplifier: Investigation of ultra-fast cross gain modulation in the presence of a second excited state", Journal of Physics D: Applied Physics, 53, 355108.

[18] Jennings, C., Ma, X., Wickramasinghe, T., Doty, M., Scheibner, M., Stinaff, E., Ware, M. (2020). "Self-assembled InAs/GaAs coupled quantum dots for photonic quantum technologies", Advanced Quantum Technologies, 3.

[19] Jung, H., Ahn, N., Klimov, V.I. (2021). "Prospects and challenges of colloidal quantum dot laser diodes", Nature Photonics, 15, 643-655.

[20] Kargozar, S., Hoseini, S.J., Brouki Milan, P., Hooshmand, S., Kim, H.W., Mozafari, M.(2020). "Quantum dots: A review from concept to clinic", Biotechnology Journal, 15, e2000117.

[21] Koley, S., Cui, J., Panfil, Y.E., Banin, U. (2021). "Coupled colloidal quantum dot molecules", Accounts of Chemical Research, 54, 1178-1188.

[22] Ledentsov, N.N., Ustinov, V.M., Egorov, A.Y., Zhukov, A.E., Maksimov, M.V., Tabatadze, I.G., Kop'ev, P.S. (1994). "Optical properties of heterostructures with InGaAs-GaAs quantum clusters", Semiconductors, 28, 832-834.

[23] Lee, I.H., Rao, V., Martin, R.M., Leburton, J.P. (2021). "Shell filling of artificial atoms within the density functional theory", In Physical Models for Quantum Dots, 103-122.

[24] Liu, L., Najar, A., Wang, K., Du, M., Liu, S. (2022). "Perovskite quantum dots in solar cells". Advanced Science, 9, 2104577.

[25] Liu, Z., Hantschmann, C., Tang, M., Lu, Y., Park, J.S., Liao, M., Liu, H. (2019). "Origin of defect tolerance in InAs/GaAs quantum dot lasers grown on silicon", Journal of Lightwave Technology, 38, 240-248.

[26] Liu, Z., Lin, C.H., Hyun, B.R., Sher, C.W., Lv, Z., Luo, B., He, J.H. (2020). "Micro-light-emitting diodes with quantum dots in display technology", Light: Science & Applications, 9, 83.

[27] Liu, H.Y., Sellers, I.R., Badcock, T.J., Mowbray, D.J., Skolnick, M.S., Groom, K.M., Beanland, R. (2004). "Improved performance of 1.3 μm multilayer InAs quantum-dot lasers using a high-growth-temperature GaAs spacer layer", Applied Physics Letters, 85(5), 704-706.

[28] Lv, Z.R., Zhang, Z.K., Yang, X.G., Yang, T. (2018). "Improved performance of 1.3-μm InAs/GaAs quantum dot lasers by direct Si doping", Applied Physics Letters, 113.

[29] Lv, S.F., Montrosset, I., Gioannini, M., Song, S.Z., Ma, J.W. (2011). "Modeling and simulation of InAs/GaAs quantum dot lasers", Optoelectronics Letters, 7, 122-125.

[30] Lüdge, K., Bormann, M.J., Malić, E., Hövel, P., Kuntz, M., Bimberg, D., Knorr, A. Schöll, E. (2008). "Turn-on dynamics and modulation response in semiconductor quantum dot lasers", Physical Review B, 78(3), 035316.

[31] Mansoori, A., Effati, S. (2019). "An efficient neurodynamic model to solve nonlinear programming problems with fuzzy parameters", Neurocomputing, 334, 125-13.

[32] Molaei, M.J. (2020). "Principles, mechanisms, and application of carbon quantum dots in sensors: A review", Analytical Methods, 12, 1266-1287.

[33] Ozaki, N., Hayashi, Y., Ohkouchi, S., Ohsato, H., Watanabe, E., Ikeda, N., Hogg, R.A. (2021). "Emission wavelength control of InAs/GaAs quantum dots using an As2 source for near-infrared broadband light source applications", Applied Physics Express, 14.

[34] Rakhlin, M., Klimko, G., Sorokin, S., Kulagina, M., Zadiranov, Y., Kazanov, D., Toropov, A. (2022). "Bright single-photon sources for the telecommunication O-band based on an InAs quantum dot with (In) GaAs asymmetric barriers in a photonic nanoantenna", Nanomaterials, 12.

[35] Razaghi, M., Izadyar, S.M., Madanifar, K.A. (2017). "Investigation of amplified spontaneous emission in quantum dot semiconductor optical amplifier in presence of second excited state", In 2017 International Conference on Numerical Simulation of Optoelectronic Devices, 37-38.

[36] Roh, J., Park, Y.S., Lim, J. Klimov, V.I. (2020). "Optically pumped colloidal-quantum-dot lasing in LED-like devices with an integrated optical cavity", Nature Communications, 11, 271.

[37] Selopal, G.S., Zhao, H., Wang, Z.M., Rosei, F. (2020). "Core/shell quantum dots solar cells, Advanced Functional Materials, 30, 1908762.

[38] Shojaeifard, A., Amroudi, A.N., Mansoori, A., Erfanian, M. (2019). "Projection recurrent neural network model: A new strategy to solve weapon-target assignment problem", Neural Processing Letters, 50, 3045-3057.

[39] Shu, Y., Lin, X., Qin, H., Hu, Z., Jin, Y., Peng, X. (2020). "Quantum dots for display applications". Angewandte Chemie International Edition, 59, 22312-22323.

[40] Sugawara, M. (1998). "Effect of carrier dynamics on quantum-dot laser performance and the possibility of bi-exciton lasing", In Physics and Simulation of Optoelectronic Devices, 3283, 88-99.

[41] Sugawara, M., Mukai, K., Nakata, Y., Ishikawa, H., Sakamoto, A. (2000). "Effect of homogeneous broadening of optical gain on lasing spectra in self-assembled In x Ga 1− x A s/G a A s quantum dot lasers", Physical Review B, 61.

[42] Urayama, J., Norris, T.B., Singh, J., Bhattacharya, P. (2001). "Observation of phonon bottleneck in quantum dot electronic relaxation", Physical review letters, 86, 4930.

[43] Wan, Y., Norman, J., Liu, S., Liu, A., Bowers, J.E. (2021). "Quantum dot lasers and amplifiers on silicon: Recent advances and future developments", IEEE Nanotechnology Magazine, 15, 8-22.

[44] Wang, J., Wang, L., Yu, S., Ding, T., Xiang, D., Wu, K. (2021). "Spin blockade and phonon bottleneck for hot electron relaxation observed in n-doped colloidal quantum dots", Nature Communications, 12.